Energy gap, excitonic, and "internal" Mn^{2+} optical transition in Mn-based II-VI diluted magnetic semiconductors

Y. R. Lee and A. K. Ramdas
Department of Physics, Purdue University, West Lafayette, Indiana 47907

R. L. Aggarwal
Francis Bitter National Magnet Laboratory and Department of Physics, Massachusetts Institute of Technology, Cambridge, Massachusetts 02139

(Received 15 January 1988)

The piezomodulated and the photomodulated reflectivity spectra of Mn-based diluted magnetic semiconductors ($Cd_{1-x}Mn_xTe$,$Zn_{1-x}Mn_xTe$,$Cd_{1-x}Mn_xSe$,$Zn_{1-x}Mn_xSe$) reveal sharp signatures associated with the excitonic transitions near the band gap. The dependence of the excitonic energy on the manganese concentration (x), on temperature (T), and, in the wurtzite structure, on the polarization with respect to the optic axis, are determined from the modulation experiments. The excitonic energy in the "hypothetical" tetrahedrally coordinated MnTe and MnSe, viewed as the end members of the alloy systems, are deduced from the x dependence of the excitonic transition. A signature associated with Mn^{2+} is observed in piezomodulated "pseudoreflection," when the energy gap is sufficiently large; its energy is insensitive to x. The absence of the Zeeman effect for the Mn^{2+} signature, in contrast to the large Zeeman effect of the excitonic feature, demonstrates that the former is an optical transition associated with the $3d^5$ shell of Mn^{2+}.

I. INTRODUCTION

The introduction of magnetic ions in semiconductors results in a fascinating class of semiconducting alloys—known as diluted magnetic semiconductors (DMS's). Due to the presence of the magnetic ions, the DMS's exhibit properties unique from both the semiconductor and the magnetic points of view.[1] In recent years Mn-based II-VI DMS's have attracted considerable attention as a result of the large exchange interaction between the band electrons and Mn^{2+}, the so-called "*sp-d* exchange interaction." The antiferromagnetic coupling between the Mn^{2+} ions underlies another equally fascinating set of phenomena exhibited by the Mn-based DMS's. Magnetization steps,[2] Raman spectrum,[3] and inelastic neutron scattering[4] associated with the energy levels of Mn^{2+} pairs; magnetic ordering[5] resulting in a spin-glass phase at low enough temperature and, at sufficiently large Mn^{2+} concentration, an observable one magnon Raman scattering[6]—the Raman antiferromagnetic resonance—these are examples of phenomena arising from this antiferromagnetic coupling. In order to fully describe the electrical and optical properties of these alloys it is essential to explore the electronic band structure of the alloys by a variety of techniques. In this context, we have made a comprehensive study of the piezomodulated and the photomodulated reflectivity and the piezomodulated transmission spectra of $Cd_{1-x}Mn_xTe$, $Zn_{1-x}Mn_xTe$, $Cd_{1-x}Mn_xSe$, and $Zn_{1-x}Mn_xSe$.[7] We have observed unique signatures for the various electronic transitions associated with energy gaps and the electronic levels associated with Mn^{2+} and impurities. We report and discuss them in the present paper.

II. EXPERIMENTAL PROCEDURE

Single crystals of the diluted magnetic semiconductors $Cd_{1-x}Mn_xTe$, $Zn_{1-x}Mn_xTe$, $Cd_{1-x}Mn_xSe$, and $Zn_{1-x}Mn_xSe$ used in this study were grown by a modified Bridgman technique. The crystal structures and the composition ranges in which the alloys can be grown in a single-crystal phase are summarized in Table I. The crystal structure of all the samples investigated was examined with x-ray diffraction. It is interesting to note that most zinc-blende crystals normally cleave along (110). No special effort was made to orient the crystallographic directions for most of the zinc-blende crystals. Samples with wurtzite symmetry were oriented with their optic axis $\hat{c}$ along the length of the sample surface. The samples were ground and polished, followed by chemical etching on both optical surfaces. The chemical etching was performed using a solution of bromine in methanol. The nominal manganese concentration of the alloys (x) was determined by electron microprobe analysis.

The spectrometer[8] used in our study consists of a tungsten ribbon lamp or a tungsten halogen lamp as a source, a Perkin-Elmer E-1 double-pass grating monochromator,[9] and an uv-enhanced Si photodiode detector. The radiation from the monochromator is partially polarized, strongly in the vertical direction below 6000 Å and in the horizontal direction above 7500 Å. The light from the monochromator was focused on the sample with an angle of incidence $\sim 6°$. The data were obtained

TABLE I. The crystal structure of Mn-based II-VI DMS's.

Alloy	Manganese concentration	Crystal structure
$Cd_{1-x}Mn_xTe$	$0<x<0.75$	zinc-blende
$Zn_{1-x}Mn_xTe$	$0<x<0.5$	zinc-blende
$Cd_{1-x}Mn_xSe$	$0<x<0.5$	wurtzite
$Zn_{1-x}Mn_xSe$	$0<x<0.35$	zinc-blende
	$0.35<x<0.5$	wurtzite

without explicitly polarizing the incident radiation for the crystals with zinc-blende structure. For wurtzite crystals, a linear polarizer was employed to produce a linearly polarized light either parallel or perpendicular to $\hat{c}$.

A glass optical cryostat enabled measurements with either liquid nitrogen or liquid helium as a coolant. The sample was mounted on a cold finger providing a thermal contact between the sample and the coolant. The sample temperature was estimated to be a few degrees higher than that of the coolant.

The piezomodulation of reflectivity or transmission spectra of DMS single crystals was accomplished by mounting the sample on a lead-zirconate-titanate piezoelectric transducer.[10] The transducer was driven by a sinusoidal electric field of about 300 V/mm rms along its thickness with an operating frequency of about 1 kHz. The sample was thus strained in the coplanar mode with a typical rms strain of the order of 10^{-5} value. For piezoreflectivity measurements, a thin sample ($t \sim 0.4$ mm) was mounted directly on one of the electrode surfaces of the transducer with Duco cement for room-temperature measurements or with vacuum grease for low temperature measurements. For piezotransmission measurements, a rectangular hole was cut in the transducer so that the radiation could be transmitted through the sample. In photomodulated reflectivity measurements, the reflectivity of the crystal was modulated by a second, intense monochromatic laser beam with a photon energy larger than the fundamental energy gap of the sample.[11] The 6328 Å radiation from a He-Ne laser or the 5145 Å radiation from an Ar^+ laser, chopped at 560 Hz, was used for producing photomodulation. A typical laser power intensity was ~ 10 mW/cm^2. A filter with a cutoff frequency lower than the laser frequency was placed in front of the detector to eliminate the laser radiation. In both piezomodulation and photomodulation the modulated signal was detected by a phase-sensitive lock-in amplifier. Data acquisition and processing were carried out with the aid of a microcomputer. The magnetoreflectance measurements were performed at the Francis Bitter National Magnet Laboratory. An optical cryostat with bottom-view fused-quartz windows was employed, the samples being immersed in pumped liquid helium at 1.3 K. The cryostat was placed in a Bitter solenoid providing high dc magnetic fields (**B**).

III. EXPERIMENTAL RESULTS AND DISCUSSIONS

The zinc-blende Mn-based DMS's belong to the space group T_d^2. They are direct band-gap semiconductors with a Γ_6 absolute conduction-band minimum separated from the Γ_8 valence-band maximum by E_g; lying below Γ_8 is the Γ_7 spin-orbit-spit valence-band maximum, all located at the center of the Brillouin zone. The wurtzite Mn-based DMS's belong to the space group C_{6v}^4 having a zone center Γ_7 absolute conduction-band minimum and valence-band maxima Γ_9, Γ_7, and Γ_7 in the order of decreasing energy; Γ_9 and the higher Γ_7 are separated due to the uniaxial crystal structure whereas the lower Γ_7 is the spin-orbit-split valence-band maximum.

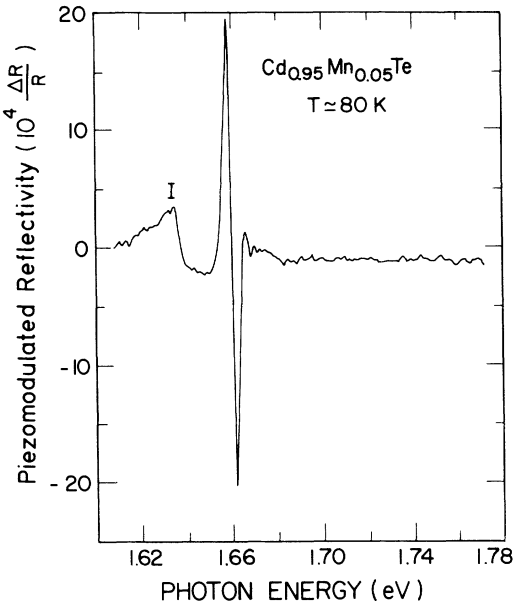

FIG. 1. Piezomodulated reflectivity spectrum of $Cd_{0.95}Mn_{0.05}Te$. Liquid nitrogen used as coolant ($T \simeq 80$ K).

A. $Cd_{1-x}Mn_xTe$ and $Zn_{1-x}Mn_xTe$

Figure 1 shows the piezomodulated reflectivity spectrum of $Cd_{0.95}Mn_{0.05}Te$ at a temperature $T \simeq 80$ K. The spectrum was recorded for energies in the vicinity of the absorption edge. The sharp feature which occurs at the photon energy $\hbar\omega = 1.660$ eV is close to the energy of the $\Gamma_8 \rightarrow \Gamma_6$ interband transition and is attributed to the free exciton. On the basis of measurements on a variety of samples we conclude that the weak feature which occurs at $\hbar\omega = 1.630$ eV is extrinsic, i.e., due to imperfections in the sample. Figure 2 shows the photomodulated

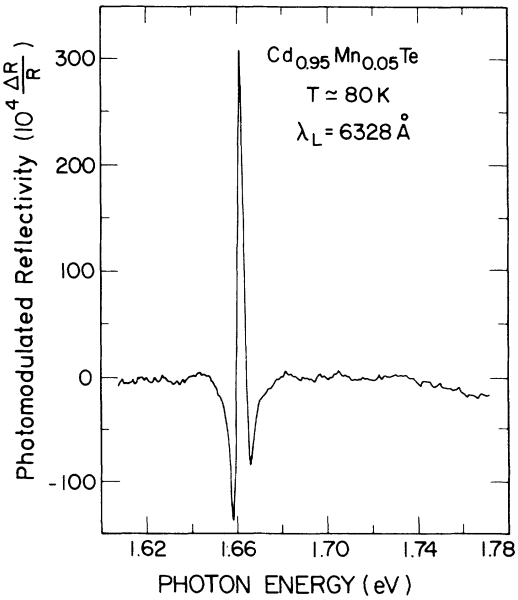

FIG. 2. Photomodulated reflectivity spectrum of $Cd_{0.95}Mn_{0.05}Te$ at $T \simeq 80$ K. Chopped 6328-Å radiation from a He-Ne laser was used to produce the photomodulation.

reflectivity spectrum at $T \simeq 80$ K for the same sample as that used for Fig. 1. Chopped 6328-Å radiation from a He-Ne laser was used to produce the photomodulation. As can be seen, a sharp signature at 1.660 eV is also observed in the photomodulated reflectivity spectrum.

The piezomodulated reflectivity spectra of a series of $Cd_{1-x}Mn_xTe$ alloys are displayed in Fig. 3. Following Camassel *et al.*,[12] we identify the peak labeled A in Fig. 3(a) for CdTe with the fundamental exciton, whereas the B and C peaks are attributed to impurities. In the spirit of virtual crystal approximation, we attribute the peaks labeled A in Figs. 3(b), 3(c), and 3(d) to the free exciton of the alloys. The results clearly show that the energy of the A peak E_A increases with x. Similar results were obtained with $Zn_{1-x}Mn_xTe$. Figure 4 shows the piezomodulated reflectivity spectra of $Zn_{1-x}Mn_xTe$ for both $x=0$ and $x=0.28$ at $T \simeq 80$ K. The sharp peak labeled A at $\hbar\omega = 2.367$ eV in Fig. 4(a) is associated with the free exciton of ZnTe, whereas the signature at $\hbar\omega = 2.553$ eV in Fig. 4(b) is associated with that of $Zn_{0.72}Mn_{0.28}Te$. In addition to the free-exciton feature, a minimum labeled Mn^{2+} appears at ~ 2.18 eV in Figs. 3(c) and 3(d) for $Cd_{1-x}Mn_xTe$ and at ~ 2.12 eV in Fig. 4(b) for $Zn_{1-x}Mn_xTe$; it is attributed to an internal transition of the Mn^{2+} ion. The feature occurs at an energy higher than that of the band gap of $Cd_{1-x}Mn_xTe$ for $x < 0.4$ and hence is obscured; but for $x > 0.4$, the larger E_g allows the feature to be manifested. In contrast, the Mn^{2+} feature is observed for all values of x in $Zn_{1-x}Mn_xTe$; the E_g of $Zn_{1-x}Mn_xTe$ is always greater than the $E_{Mn^{2+}}$

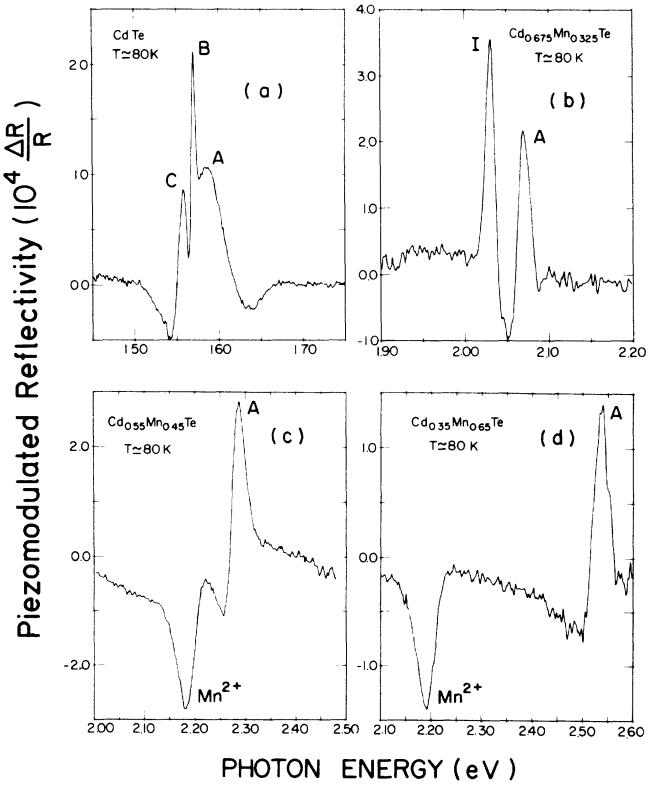

FIG. 3. Piezomodulated reflectivity spectra of $Cd_{1-x}Mn_xTe$: (a) $x=0$, (b) $x=0.325$, (c) $x=0.45$, and (d) $x=0.65$.

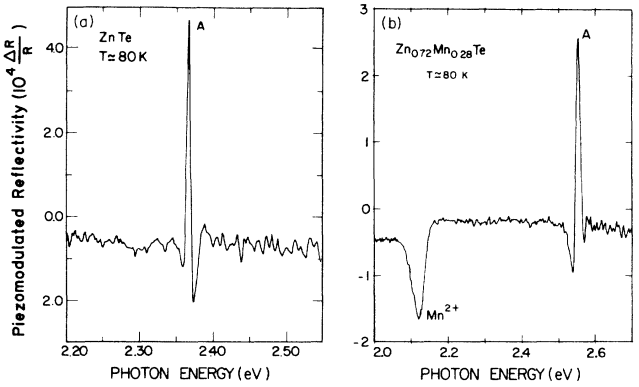

FIG. 4. Piezomodulated reflectivity spectrum of ZnTe and $Zn_{0.72}Mn_{0.28}Te$ at $T \simeq 80$ K.

allowing the Mn^{2+} feature to be visible for all x. In Fig. 5 we summarize the variation of E_A and $E_{Mn^{2+}}$ as a function of x in both $Cd_{1-x}Mn_xTe$ and $Zn_{1-x}Mn_xTe$ at three different temperatures. The results show that E_A varies linearly with x throughout the composition range. The linear dependence of E_A with x for the temperatures measured is summarized in Table II. Viewed as an end member of $Cd_{1-x}Mn_xTe$ and $Zn_{1-x}Mn_xTe$, the values of E_A at $x=1$ in Table II can be attributed to the free-exciton energy of the "hypothetical" zinc-blende MnTe. It is to be noted that MnTe crystallizes in the hexagonal NiAs structure; it has an absolute conduction-band minimum at the L point of its Brillouin zone which lies 1.3 eV above the valence band whereas it has an indirect gap of 0.35 eV.[13] It is interesting to note that the value of $E_A(x=1)$ deduced from both $Cd_{1-x}Mn_xTe$ and $Zn_{1-x}Mn_xTe$ are in close agreement for all three temperatures. The value of $E_{Mn^{2+}}$, however, shows no noticeable x dependence. The feature labeled "I" in Fig. 3(b) is attributed to imperfections in the sample. Interpretation of the "Mn^{2+}" and the I features will be given in Secs. III E and III F, respectively.

We note that the I and Mn^{2+} features shown in the piezomodulated reflectivity spectra should be regarded as arising from a "pseudoreflection"; more specifically, they occur in a spectral region where the sample is transparent, allowing radiation to pass through. The transmitted radiation is then reflected from the back surface. The signature actually arises from a piezomodulation of an absorption process. This deduction is based upon the following.

(i) Features I and Mn^{2+} can only be observed in "piezomodulated reflectivity" measurements if the sample back surface is well polished. They disappear when the sample back surface is made rough.

(ii) In piezomodulated transmission measurements, features I and Mn^{2+} appear whereas those associated with the free exciton, which occurs in a low transmission spectral range, disappear.

(iii) Neither the I nor the Mn^{2+} feature is observed in photomodulated reflectivity measurements irrespective of the nature of the back surface. This is understandable since in photomodulation experiments the reflected radia-

TABLE II. Energy of the A exciton, E_A (eV), in $Cd_{1-x}Mn_xTe$ and $Zn_{1-x}Mn_xTe$ as a function of x.

	$Cd_{1-x}Mn_xTe$		$Zn_{1-x}Mn_xTe$	
T (K)	$E_A(x)$	$E_A(x=1)$	$E_A(x)$	$E_A(x=1)$
300	$1.528+1.316x$	2.844	$2.271+0.518x$	2.789
80	$1.586+1.501x$	3.087	$2.365+0.721x$	3.086
10	$1.595+1.592x$	3.187	$2.376+0.820x$	3.196

tion is modulated by an ac space charge field near the sample surface. Such an electric field, in general, has a depth of a few micrometers, not enough to produce a significant modulated transmission signal. In contrast, in piezomodulated reflectivity experiments the entire sample experiences an alternating stress and therefore both the reflected and the transmitted light beams are modulated.

The data presented in Fig. 5 also indicate two interesting aspects of the temperature coefficient of E_A (dE_A/dT).

(i) The value of $|dE_A/dT|$ increases linearly with increasing x for the temperature interval 80–300 K and is given by

$$|dE_A/dT| = 10^{-4}(2.6+8.8x)\ \text{eV/K} . \quad (1)$$

This result is in good agreement with that deduced from wavelength-modulated reflectivity measurement.[14] For the temperature interval 10–80 K, $|dE_A/dT|$ appears to be independent of x for $x \leq 0.1$, while for larger x it increases "almost" linearly with x. A similar behavior was observed in electroreflectance.[15] Variation of lattice constant with temperature and electron-phonon interaction have been proposed in the literature[16] to account for the temperature dependence of the energy gap. Based on the information currently available, such as the variation of lattice parameters[17] and phonon frequencies[18] with x, one cannot, however, fully explain the linear dependence behavior of dE_A/dT with x in Mn-based II-VI DMS. Although Bottka *et al.*[15] have speculated that in $Cd_{1-x}Mn_xTe$ the concentration of vacancies would increase with x and in turn soften the lattice vibrations, so far there are no direct experimental results to support this speculation.

(ii) The variation of the energy band gap E_g with temperature T of a classical semiconductor can be empirically represented by[19]

$$E_g(T) = E_0 - aT^2/(T+b) , \quad (2)$$

where E_0 is the energy band gap at $T=0$ K and a and b are constants. Equation (2) shows that the value of $|dE_g/dT|$ should be larger for higher T. For example, the value of $|dE_g/dT|$ in units of 10^{-4} eV/K for pure CdTe decreases from 5.4 at 800 K (Ref. 20) to 2.3 at 77 K.[21] Our measurements on $Cd_{0.3}Mn_{0.7}Te$ show that $|dE_A/dT|$ is 8.5 and 10.4 for the temperature intervals 80–300 and 10–80 K, respectively. We speculate that this anomalous temperature dependence E_g in $Cd_{1-x}Mn_xTe$ for the larger x is related to the magnetic ordering of the alloys[5,7] with Mn content. The temperature variation of E_A in $Zn_{1-x}Mn_xTe$ shows a behavior similar to that observed in $Cd_{1-x}Mn_xTe$ (see Table III). These results are in agreement with those obtained from absorption measurements.[22] In contrast, the temperature coefficient of the Mn^{2+} transition, $dE_{Mn^{2+}}/dT$, has the same value for both temperature intervals at which the observations were made, viz., -4.5×10^{-4} eV/K for both $Cd_{1-x}Mn_xTe$ and $Zn_{1-x}Mn_xTe$. The anomalies in $dE_g(x)/dT$ for large x noticed for $Cd_{1-x}Mn_xTe$ and $Zn_{1-x}Mn_xTe$ are discussed in Sec. III D along with the similar but pronounced effects shown by $Zn_{1-x}Mn_xSe$.

In addition to the $\Gamma_8 \rightarrow \Gamma_6$ interband transition, we have also investigated the photomodulated reflectivity in the spectral range where the optical transition from the spin-orbit Γ_7 valence band to the Γ_6 conduction band in $Cd_{1-x}Mn_xTe$ occurs. Figure 6 shows the photomodulated reflectivity spectrum of CdTe at $T \simeq 80$ K. The spectrum was recorded for photon energies in the vicinity of $E_g + \Delta_{s.o.}$. The feature at 2.503 eV is attributed to the

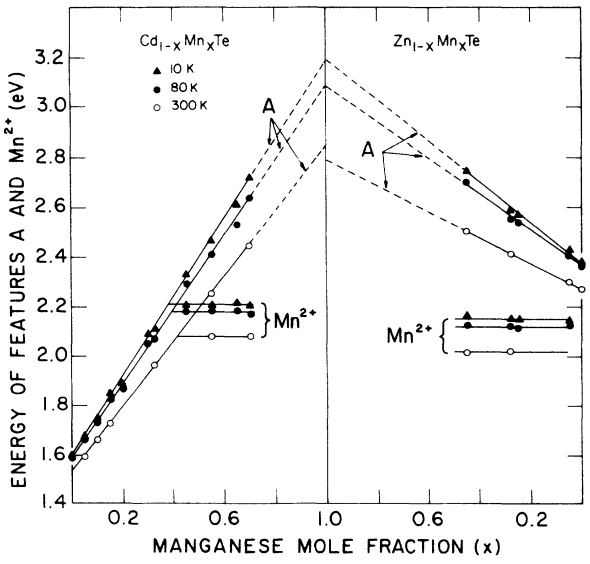

FIG. 5. Energies of the A and Mn^{2+} features as a function of x, the manganese molar fraction, in $Cd_{1-x}Mn_xTe$ and $Zn_{1-x}Mn_xTe$.

TABLE III. The temperature variation of E_A, dE_A/dT, in $Zn_{1-x}Mn_xTe$

	dE_A/dT (10^{-4} eV/K)		
T (K)	$x=0.05$	$x=0.28$	$x=0.45$
80–300	−4.9	−6.4	−8.8
10–80	−2.0	−5.1	−8.3

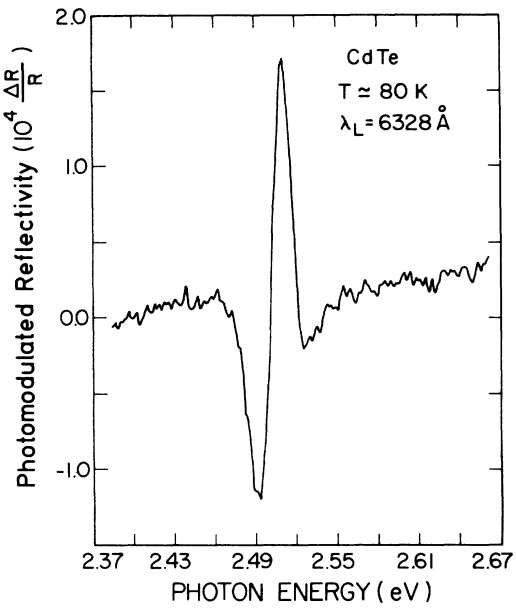

FIG. 6. Photomodulated reflectivity spectrum of CdTe at $T \simeq 80$ K. The spectrum was recorded for photon energies in the vicinity of $E_g + \Delta_{s.o.}$.

transition from the Γ_7 valence-band maximum to the Γ_6 conduction minimum. Our measurements yield $\Delta_{s.o.} = 0.917$ eV for CdTe in good agreement with that in the literature.[23] The photomodulated reflectivity spectrum of $Cd_{0.99}Mn_{0.01}Te$ at $T \simeq 80$ K (Fig. 7) shows a feature at 2.546 eV, again associated with the $\Gamma_7 \rightarrow \Gamma_6$ transition. We deduce $\Delta_{s.o.} = 0.947$ eV for $x = 0.01$, a value larger than that for CdTe in agreement with the reflectivity results.[24,25]

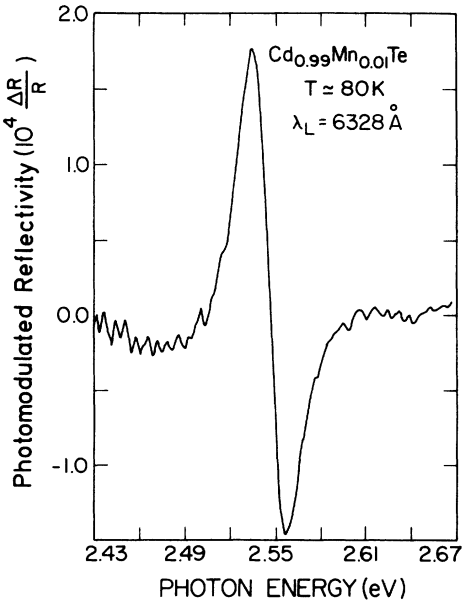

FIG. 7. Photomodulated reflectivity spectrum of $Cd_{0.99}Mn_{0.01}Te$ at $T \simeq 80$ K. The spectrum was recorded for photon energies in the vicinity of $E_g + \Delta_{s.o.}$.

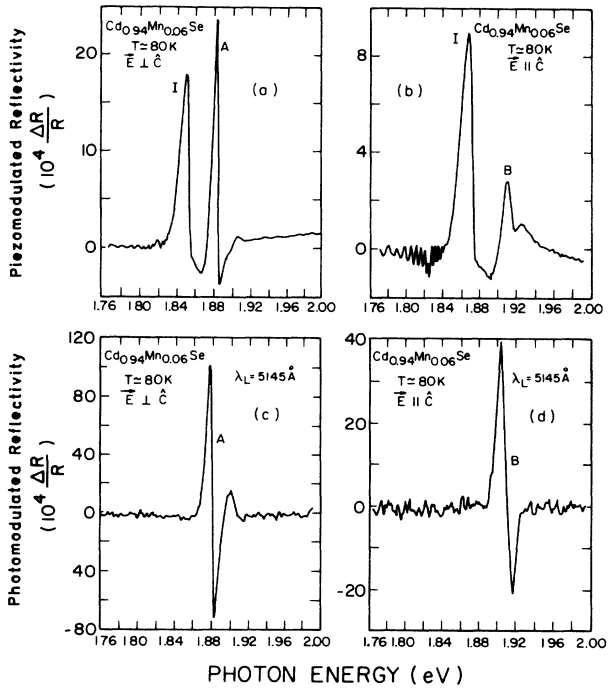

FIG. 8. Piezomodulated and photomodulated reflectivity spectra of $Cd_{0.94}Mn_{0.06}Se$ at $T \simeq 80$ K.

B. $Cd_{1-x}Mn_xSe$

The free-exciton features associated with the interband transitions at the Γ point in $Cd_{1-x}Mn_xSe$ are labeled as *A*, *B*, and *C* corresponding to the transitions to the Γ_7 conduction band from the Γ_9 valence band, the crystal-field-split Γ_7 valence band, and the lower spin-orbit-split Γ_7 valence band, respectively. The *A* exciton is observable only for $\mathbf{E} \perp \hat{\mathbf{c}}$, where $\mathbf{E}$ is the electric vector and $\hat{\mathbf{c}}$ the optic axis; on the other hand, the *B* and *C* excitons can be observed for both $\mathbf{E} \perp \hat{\mathbf{c}}$ and $\mathbf{E} \parallel \hat{\mathbf{c}}$.

Figure 8 displays the piezomodulated and photomodulated reflectivity spectra for $Cd_{0.94}Mn_{0.06}Se$ at $T \simeq 80$ K in the spectral range where the *A* and *B* excitons occur. It should be noted that all the wurtzite crystals studied were oriented with $\hat{\mathbf{c}}$ lying in the sample surface; incident light is polarized either parallel or perpendicular to $\hat{\mathbf{c}}$ as indicated in the spectra. The piezomodulation of reflectivity was achieved, as for the cubic DMS's, by coplanar ac stress applied to the optical surface, whereas the photomodulation was produced by the space charge field, caused by a chopped 5145-Å radiation from an Ar^+-ion laser. The signatures are appropriately labeled as *A* and *B* excitons. Although both *A* and *B* excitons are allowed for $\mathbf{E} \perp \hat{\mathbf{c}}$, only the *A* exciton feature is dominant in both piezomodulated and photomodulated reflectivity spectra. In $\mathbf{E} \parallel \hat{\mathbf{c}}$ only the *B* exciton was observed. The additional features labeled *I* in Figs. 8(a) and 8(b) are attributed to imperfections in the sample. The energy of *I*, E_I, is 1.868 eV for $\mathbf{E} \parallel \hat{\mathbf{c}}$, and 1.856 eV for $\mathbf{E} \perp \hat{\mathbf{c}}$. The oscillation pattern at low energies in Figs. 8(a) and 8(b) is due to channeling, which is characteristic of a plane-parallel plate in its transparent region. For higher values of x, the *A* and *B* excitons move to higher ener-

gies, as shown both in Fig. 9(a) and 9(b), where we show the piezomodulated reflectivity spectra of $Cd_{0.52}Mn_{0.48}Se$ at $T \simeq 10$ K. In addition, a minimum labeled Mn^{2+} is observed at $\hbar\omega = 2.338$ eV for both $\mathbf{E} \perp \hat{c}$ [Fig. 9(a)] and $\mathbf{E} \| \hat{c}$ [Fig. 9(b)]. This feature is attributed to an internal transition of Mn^{2+} in the tetrahedrally coordinated environment. Figure 10 summarizes the variation of both E_A and E_B as a function of x for three different temperatures. It is clear that E_A and E_B increase linearly with x throughout the composition range. The linear dependence of E_A and E_B with x is summarized in Table IV. Viewed as an end member of $Cd_{1-x}Mn_xSe$, the value of E_A ($\simeq E_B$) at $x = 1$ can be attributed to the free-exciton energy of MnSe with a tetrahedral coordination. It is interesting to note that both E_A and E_B have an identical temperature dependence. The value of dE_A/dT (dE_B/dT) varies linearly with x for the temperature interval 10–80 K and is given by

$$|dE_A/dT| = |dE_B/dT| = 10^{-4}(1.5+11.0x) \text{ eV/K} . \quad (3)$$

For the temperature interval 80–300 K, $|dE_A/dT|$ ($|dE_B/dT|$) is practically independent of x for $x < 0.1$ and is "almost" linear with x for $x > 0.1$.

The value of $|dE_{Mn^{2+}}/dT|$ in $Cd_{1-x}Mn_xSe$ for the temperature interval 10–80 K is 2.9×10^{-4} eV/K, similar to that in $Zn_{1-x}Mn_xSe$ discussed in the next section but somewhat smaller than that in $Cd_{1-x}Mn_xTe$ and $Zn_{1-x}Mn_xTe$. This may be attributed to the effect of the replacement of Te by Se. The energy difference between E_A and E_B, Δ, is often attributed to the crystal anisotropy. Table V summarizes the value of Δ for all the samples of $Cd_{1-x}Mn_xSe$ studied. In contrast to the observation made by Stankiewicz[26] who reported that Δ decreased linearly with x, our results show, within the experimental error, that the value of Δ is constant for smaller x and becomes smaller for larger x. The value of Δ does not show noticeable temperature dependence except for highest x.

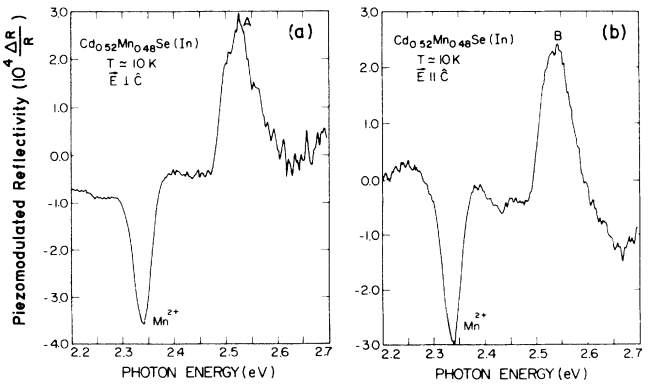

FIG. 9. Piezomodulated reflectivity spectrum of $Cd_{0.52}Mn_{0.48}Se$ at $T \simeq 10$ K. (a) $\mathbf{E} \perp \hat{c}$. (b) $\mathbf{E} \| \hat{c}$.

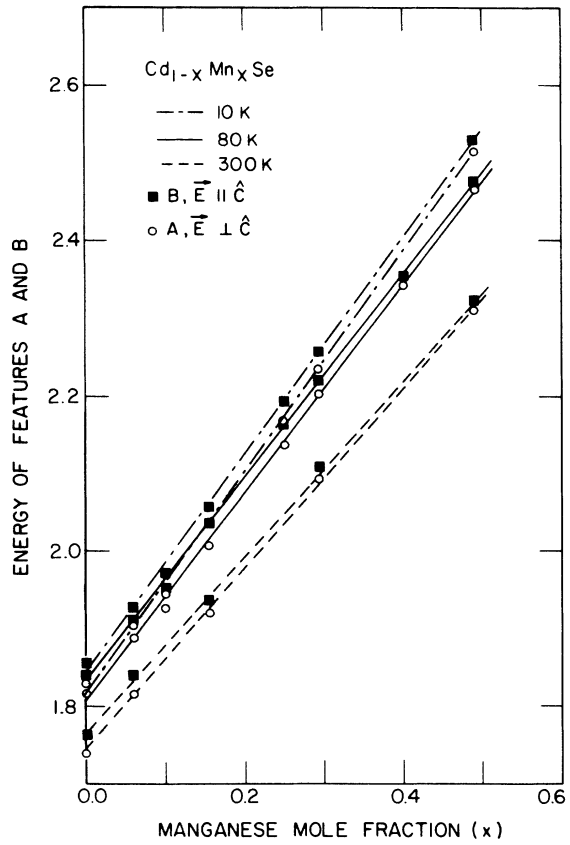

FIG. 10. Energies of A and B excitons in $Cd_{1-x}Mn_xSe$ as a function of x.

C. $Zn_{1-x}Mn_xSe$

$Zn_{1-x}Mn_xSe$ alloys have zinc-blende crystalline structure for $0 \leq x < 0.35$ and wurtzite structure for higher values of x. Figure 11 shows the piezomodulated reflectivity spectrum of $Zn_{0.78}Mn_{0.22}Se$ at $T \simeq 10$ K. The peak at $\hbar\omega = 2.89$ eV is the signature of the free exciton, whereas the feature labeled Mn^{2+} at 2.28 eV is again associated with a Mn^{2+} internal transition. Figure 12 shows the variation of the free-exciton energy of $Zn_{1-x}Mn_xSe$ as a function of x. It is unusual compared to that in $Cd_{1-x}Mn_xTe$, $Zn_{1-x}Mn_xTe$, and $Cd_{1-x}Mn_xSe$. The value of E_A in $Zn_{1-x}Mn_xSe$ initially decreases and then increases with x. This anomalous behavior was also noticed in reflectivity[27] and photoluminescence.[28] The origin of this anomaly is discussed in the following section. For $x > 0.35$, the free exciton shows dichroism as the crystalline structure becomes wurtzite. As in $Cd_{1-x}Mn_xSe$, Δ appears to be smaller

TABLE IV. The dependence of the energies of the A and B excitons, i.e., of E_A and E_B with manganese concentration in $Cd_{1-x}Mn_xSe$.

T (K)	E_A (eV)	E_B (eV)
300	$1.743+1.16x$	$1.766+1.14x$
80	$1.807+1.34x$	$1.833+1.31x$
10	$1.817+1.42x$	$1.841+1.40x$

TABLE V. The x and T dependence of $E_B - E_A = \Delta$ in $Cd_{1-x}Mn_xSe$.

x	Δ (meV) 300 K	80 K	10 K
0	24	23	23
0.06	23	23	23
0.1		25	24
0.155	24	30	20
0.25		25	24
0.3	19	21	20
0.4		16	
0.49	10	10	14

for large values of x. In addition to the 2.2-eV Mn^{2+} transition, we observe a new minimum at $\hbar\omega \sim 2.8$ eV for $x > 0.35$ and also attribute it to a Mn^{2+} internal transition. Both 2.2- and 2.8-eV transitions show small but noticeable x dependence, but no dichroism.

D. Effect of the s-d and p-d exchange interaction on the energy gap of Mn-based DMS's

As we have seen above, the temperature dependence of the energy of the exciton shows two anomalous features, viz. (i) an "apparent" additional blue shift of the fundamental energy gap at low temperatures for large x and (ii) a nonlinear dependence of the energy gap on x for low x in $Zn_{1-x}Mn_xSe$.

Diouri *et al.*[29] and Bylsma *et al.*[28] have considered the interaction of magnetization with the energy band states in the absence of the magnetic field. For the alloy in its paramagnetic phase, as a result of a second-order perturbation, the exchange interaction between the Mn^{2+} ion and the band electrons (the so-called s-d and p-d interactions) gives rise to a negative and a positive correction to the energy of the conduction and valence bands, respectively, and causes a red shift of the energy gap. When the alloy enters the antiferromagnetic or spin-glass phase, the effect of the exchange interaction decreases, in turn removing this red shift, and producing an apparent additional blue shift of the energy gap at low temperatures. The energy correction in the paramagnetic phase can be expressed in terms of an x-dependent magnetic susceptibility (χ) given by

$$\Delta E(x,T) = -\beta\chi T \ , \tag{4}$$

where β is an adjustable parameter. For $Zn_{1-x}Mn_xSe$, Bylsma *et al.*[28] have shown that $\Delta E(x,T)$ has a pronounced ninimum at $x \sim 0.1$ for low T. From Eqs. (2) and (4), the x and T dependence of the energy gap, $E_g(x,T)$, can be expressed by[28]

$$E_g(x,T) = E_0 + \alpha x - \frac{aT^2}{T+b} - \beta\chi T \ , \tag{5}$$

where E_0 is the energy gap of ZnSe at $T = 0$ K and α is a constant. For $Zn_{1-x}Mn_xSe$, since αx is smaller than $\beta\chi T$ for low x, after the effect of polytype and temperature dependence have been removed, the energy gap as a function of x shows a bowing at low x, as shown in Fig. 12. In $Cd_{1-x}Mn_xTe$ such effects are much less pronounced.

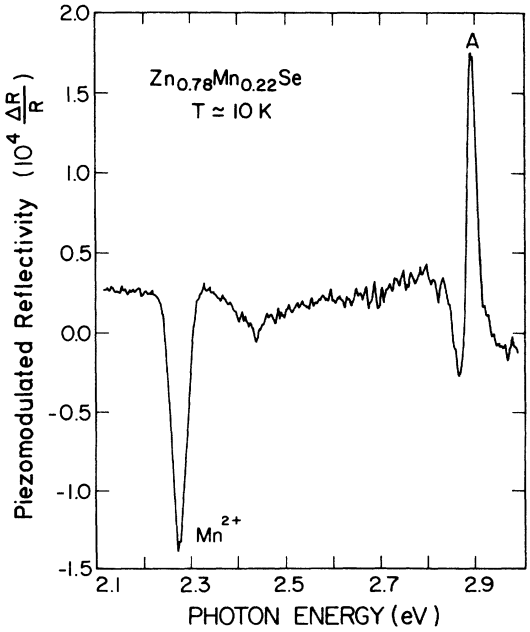

FIG. 11. Piezomodulated reflectivity spectrum of $Zn_{0.78}Mn_{0.22}Se$ at $T \simeq 10$ K.

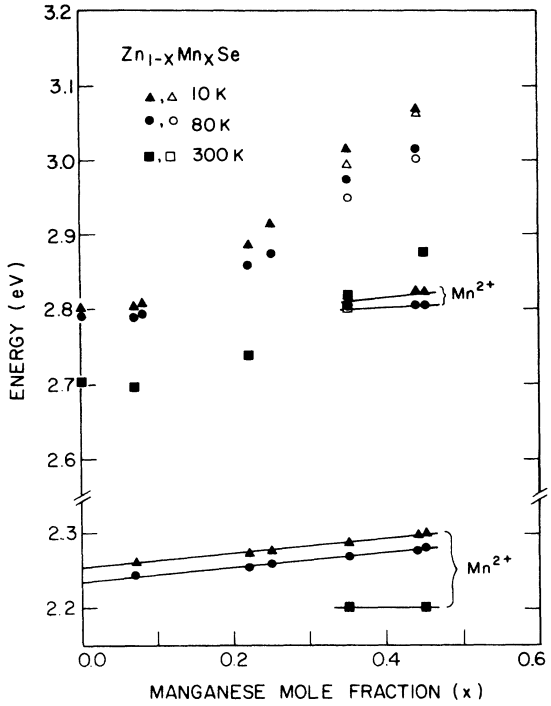

FIG. 12. The variation of free-exciton and Mn^{2+} internal transition energies of $Zn_{1-x}Mn_xSe$ as a function of x.

E. Mn^{2+} transition in Mn-based II-VI DMS's

As we mentioned earlier in this section, the piezomodulated reflectivity spectra of $Cd_{1-x}Mn_xTe$ ($x > 0.42$), $Cd_{1-x}Mn_xSe$ ($x > 0.45$), $Zn_{1-x}Mn_xTe$, and

$Zn_{1-x}Mn_xSe$ exhibit a signature labeled Mn^{2+} in the vicinity of 2.2 eV when the fundamental band gap exceeds 2.2 eV. The feature is attributed to an electronic transition of Mn^{2+}. In order to account for the 2.2-eV optical transition of Mn^{2+} observed in the Mn-based II-VI DMS's, two possible mechanisms have been proposed in the literature.

(i) The first model emphasizes the localized nature of the Mn^{2+} levels with focus on the ligand fields. According to this model, the $3d^5$ electrons of the Mn^{2+} ion in a crystal are highly localized and subject to an electrostatic field originating from the surrounding ligands. Such a "crystalline field" destroys the spherical symmetry of atomic Mn^{2+}. As a result, in the tetrahedrally coordinated environment, the first two atomic states of the $3d^5$ shell of Mn^{2+} ion split into the following:

$$^6S(L=0)\rightarrow {}^6A_1$$

for the ground state and

$$^4G(L=4)\rightarrow {}^4A_1+{}^4E+{}^4T_1+{}^4T_2$$

for the first excited free-electron state. The 2.2-eV feature of Mn^{2+} is attributed to a transition from the $^6A_1(^6S)$ symmetric ground state of the $3d^5$ configuration to the lowest crystal-field-split $^4T_1$ component of the first excited state (^4G) in which one of the $3d^5$ electrons has antiparallel spin.[30] Figure 13 shows the energy levels schematically according to this model. Also included are the other crystal-field-split levels $^4T_2$ and $^4A_1+{}^4E$. The energies of the crystal-field-split levels are characterized by an appropriate crystal-field parameter selected by comparison with experiments.

(ii) The second model views the $3d^5$ electrons of Mn^{2+} as forming a band lying ~ 3.5 eV below the Γ_8 valence-band maximum and hybridized strongly with Te $5p$ states. This location is deduced from photoemission measurements.[31,32] When an electron is added to Mn^{2+} from the Γ_8 valence-band maximum, a Mn^+ $3d^6$ band is formed[33] in which one of the electrons has antiparallel spin. It was estimated[33] that the energy required for adding an extra electron to the Mn^{2+} ion is ~ 5.8 eV. Therefore the $3d^6$ of Mn^+ band should lie ~ 2.3 eV above the Γ_8 valence-band maximum. The Mn^{2+} transition is then interpreted as the $\Gamma_8\rightarrow 3d^6$ optical transition [Fig. 13(b)].

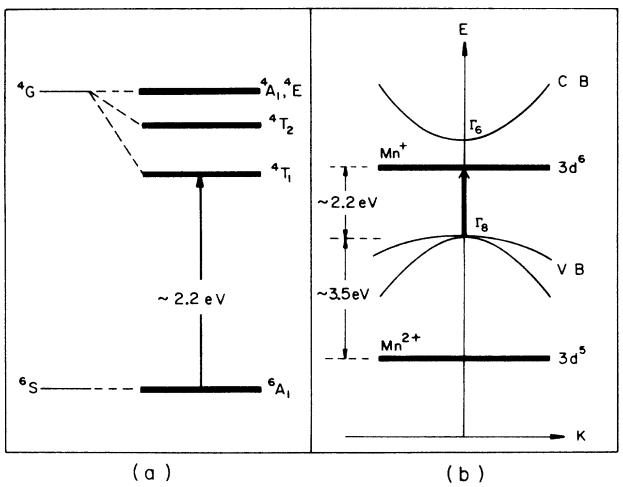

FIG. 13. Schematic diagram showing the initial and final states for the 2.2-eV transition in Mn-based II-VI DMS's, including (a) crystal-field-split $3d^5$ levels of the Mn^{2+} ion, and (b) the conduction band (CB) and valence band (VB) at the Γ point of a zinc-blende structure and the unoccupied $3d^6$ level within the band gap.

The two alternative models for the 2.2 eV transition of Mn^{2+} in the DMS can be tested on the basis of experimental results they predict. (1) The Mn^{2+} electron exchange constant $N_0\beta$ characterizing the Γ_8 valence-band maximum is known to be very large (~ 1 eV), which results in a large Zeeman splitting into $+\frac{3}{2}$, $+\frac{1}{2}$, $-\frac{1}{2}$, and $-\frac{3}{2}$ subbands. If the model in Fig. 13(b) is the correct microscopic picture for the transition, clearly a large Zeeman splitting in an external magnetic field is to be expected for the transition. This should be comparable to that observed for free excitons.[2,34] (2) The large Zeeman splitting expected from Fig. 13(b) also implies a large Faraday rotation associated with the 2.2-eV transition. (3) The $\Gamma_8\rightarrow 3d^6$ optical transition in Fig. 13(b) should lead to a corresponding onset of "hole" photoconductivity. In contrast, Fig. 13(a) predicts a small Zeeman effect, very little influence on Faraday rotation, and no photoconductivity associated with the 2.2 eV transition.

In this section we present the results on the effects of the external magnetic field on the ~ 2.2-eV Mn^{2+} optical transition and their implications in the context of the tests proposed above.

Reflectivity spectra of $Zn_{0.72}Mn_{0.28}Te$, $Cd_{0.59}Mn_{0.42}Te$, $Cd_{0.52}Mn_{0.28}Se$, and $Zn_{0.55}Mn_{0.45}Se$ were studied with dc magnetic fields **B** up to 15.58 T.[35] The magnetoreflectivity spectra were measured with **B** along [110] for $Zn_{0.72}Mn_{0.28}Te$ and $Cd_{0.58}Mn_{0.42}Te$ and normal to $\hat{\mathbf{c}}$ for $Cd_{0.52}Mn_{0.48}Se$ and $Zn_{0.55}Mn_{0.45}Se$. The spectra were recorded in the Faraday geometry.

Figure 14 shows the magnetic-field dependence of the excitonic feature and the Mn^{2+} transition in $Zn_{0.72}Mn_{0.28}Te$. We note that, in the Faraday geometry with $\mathbf{B}\|\hat{\mathbf{z}}$ and incident light polarized as $\hat{\sigma}_\pm=(1/\sqrt{2})(\hat{\mathbf{x}}\pm i\hat{\mathbf{y}})$ where $\hat{\mathbf{x}}$, $\hat{\mathbf{y}}$, and $\hat{\mathbf{z}}$ form a right-handed coordinate system and the exciton splits into four components: a and b observed in $\hat{\sigma}_+$, and c and d in $\hat{\sigma}_-$. It has been well established[2] that a and d originate from the $-\frac{3}{2}$ and $+\frac{3}{2}$ valence bands, whereas b and c have $-\frac{1}{2}$ and $+\frac{1}{2}$ valence bands as their initial states. As is evident, the a and d components have undergone a huge shift from the zero field position. The Mn^{2+} transition, in contrast, shows no observable Zeeman splitting. The enormous Zeeman splitting of the free exciton traced to the Mn^{2+} band electron exchange interaction is clearly demonstrated; in contrast, the absence of any observable Zeeman shift in the Mn^{2+} transition in either the $\hat{\sigma}_+$ or $\hat{\sigma}_-$ polarization is equally conspicuous. The results for the other DMS crystals examined also show the large exchange-induced Zeeman splitting for the free exciton and no observable splitting for the Mn^{2+} feature.

It is thus clear that the magnetoreflectivity results favor the model represented by Fig. 13(a), not that in Fig.

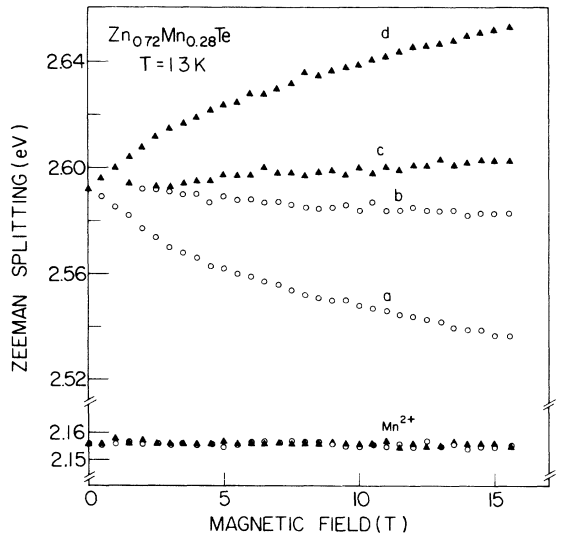

FIG. 14. Magnetic-field dependence of the energies for the Zeeman components of the free exciton and the 2.2-eV transition in $Zn_{0.72}Mn_{0.28}Te$ at 1.3 K. Solid triangles and open circles denote the transitions for $\hat{\sigma}_-$ and $\hat{\sigma}_+$ polarization, respectively.

13(b). On the scale of the results shown in Fig. 14 the Zeeman effect for the transition represented by the ${}^6A_1 \rightarrow {}^4T_1$ transition will escape observation in view of the large width of Mn^{2+} transition and g factors of the order ~ 1 or 2 expected for the excited and ground states.

Calas *et al.*[36] have reported photoconductivity results for $Cd_{0.27}Mn_{0.73}Te$. In addition to the intrinsic photoconductivity they observed photoresponse at lower energies associated with the "band tails." A pronounced dip appeared in the spectrum precisely at the Mn^{2+} transition energy. The dip is caused by the competing optical transition of Mn^{2+} which clearly does *not* produce free carriers if the model in Fig. 13(a) is correct; thus the photoconductivity results also rule out the $\Gamma_8 \rightarrow 3d^6$ interpretation. Wei and Zunger,[37] however, have estimated that the energy required for adding an extra electron to the Mn^{2+} ion should be ~ 5.5 eV; according to them the $3d^6$ band lies ~ 2.0 eV above the Γ_8 valence-band maximum. They then attribute the 2.0-eV peak preceding the 2.2-eV dip observed in the photoconductivity spectrum to the $\Gamma_8 \rightarrow 3d^6$ excitation. They further argue that the lack of Zeeman splitting for Mn^{2+} feature in our magnetoreflectivity results is due to the band overlap of $\Gamma_8 \rightarrow 3d^6$ and ${}^6A_1 \rightarrow {}^4T_1$ transitions. Their interpretations seem to suggest that these two independent optical processes occur at about the same energy. In contrast, Ehrenreich *et al.*[38] have calculated that the energy separation between $3d^5$ and $3d^6$ bands is 7.0 eV for $Cd_{0.9}Mn_{0.1}Te$. This implies that the $3d^6$ band should be within the conduction band even for $x > 0.4$. Recently, Franciosi *et al.*[39] have shown that in $Cd_{1-x}Mn_xTe$ the $3d^6$ Mn^+ band is located at ~ 4 eV above the Fermi level. In view of the fact that the Fermi level coincides with the valence-band maximum for p-type semiconductors, the $\Gamma_8 \rightarrow 3d^6$ interpretation for the 2.2- (or 2.0-) eV feature of Mn^{2+} should be ruled out.

Furthermore, additional experimental observations on Mn-based DMS indirectly support the model in Fig. 13(a), not the one in Fig. 13(b). (i) The dispersion of the Faraday rotation studied by Bartholomew *et al.*[40] gives no indication of any anomaly near the 2.2-eV transition of Mn^{2+}. (ii) The piezoreflectivity spectra of Mn-based DMS's showing opposite signs of the Mn^{2+} and A features are a clear indication that the energy of the 2.2-eV transition decreases with increasing compression whereas the energy gap increases with compression. This is consistent with the hydrostatic pressure measurements on $Cd_{1-x}Mn_xTe$ (Refs. 41 and 42) in which the Mn^{2+} transition shifts to lower energies with increasing hydrostatic compression, while for the energy gap it increases with compression. The crystal-field model of Mn^{2+} (Ref. 30) also shows that the energy of ${}^4T_1$ state decreases with increasing compression and increasing crystal field. (iii) For wurtzite DMS's [$Cd_{1-x}Mn_xSe$ and $Zn_{1-x}Mn_xSe$ ($x > 0.35$)], as a result of the crystal-field splitting of the Γ_8 valence band, the Mn^{2+} transition may be expected to show a corresponding splitting if the model in Fig. 13(b) is correct. Our results, however, show no indication for such an effect.

We can thus state that all experimental evidence favors this intra-Mn^{2+}-level transition over the $\Gamma_8 \rightarrow 3d^6$ interpretation.

As pointed out in Sec. III C, we have observed a second minimum at ~ 2.8 eV in $Zn_{1-x}Mn_xSe$ for $x > 0.35$. A similar optical transition was also observed in the absorption measurements in $Zn_{1-x}Mn_xSe$ (Ref. 43) and in ZnS:Mn.[44] We also attribute this feature to the intra-Mn-level transition, although the states involved in the transition have not been identified yet.

In a detailed absorption study made by Becker and coworkers[43,45] using very thin $Zn_{1-x}Mn_xTe$ and $Zn_{1-x}Mn_xSe$ samples, additional intraion Mn^{2+} transitions were observed. Besides the ${}^6A_1({}^6S) \rightarrow {}^4T_1({}^4G)$ transition, they have observed signatures associated with ${}^6A_1({}^6S) \rightarrow {}^4T_2({}^4G)$ and ${}^6A_1({}^6S) \rightarrow {}^4A_1, {}^4E({}^4G)$.

It has been pointed out in Sec. III A that features appearing below the free-exciton energy in a piezomodulated reflectivity spectrum are a result of pseudoreflection; they originate from piezomodulated transmission. In a piezomodulated-transmission measurement, the quantity which dominates a spectral structure is the one produced by $\Delta\alpha$, the change in the absorption coefficient caused by the applied stress. Failure to observe features associated with ${}^6A_1({}^6S) \rightarrow {}^4T_2({}^4G)$ and ${}^6A_1({}^6S) \rightarrow {}^4A_1, {}^4E({}^4G)$ transitions can be attributed to a small change in absorption coefficient associated with these transitions.

F. Defects in $Cd_{1-x}Mn_xTe$

Impurities and structural defects (interstitials, vacancies, and their complexes) are the common defects in semiconductors. The electronic energy levels associated with defects are often located in the energy gap. Therefore, optical measurements with photon energies smaller than the fundamental energy gap allow us to explore the transitions associated with these levels.

In piezomodulated reflectivity experiments, as a result

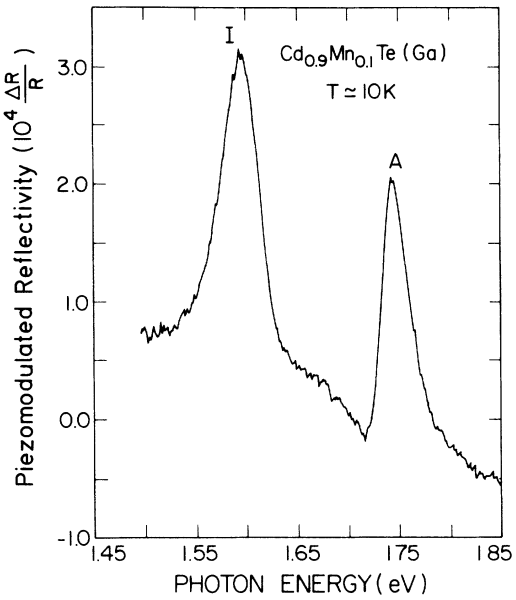

FIG. 15. Piezomodulated reflectivity spectrum of Ga-doped $Cd_{0.9}Mn_{0.1}Te$ at $T \simeq 10$ K.

of pseudoreflection, we have observed signatures appearing at energies below the free-exciton features of $Cd_{1-x}Mn_xTe$ for $x < 0.45$; these features are also observed in piezomodulated transmission measurements. We attribute them to the defects in the alloy. Samples studied are either p type, but not intentionally doped, or n-type Ga doped. Figure 15 shows the piezomodulated reflectivity spectrum of $Cd_{0.9}Mn_{0.1}Te$:Ga at $T \simeq 10$ K. The feature labeled A at 1.750 eV is attributed to the free exciton whereas the feature labeled I at 1.600 eV corresponds to a defect level in the energy gap. In CdTe an energy level associated with group-III or group-VII donors has been commonly observed within the band gap,[46] located about 0.14–0.17 eV above the valence band; it has been attributed to the group-III or group-VII donor bound to a Cd vacancy. It appears the feature I, about 0.15 eV below the free-exciton feature, in Fig. 15 is also due to such a Cd vacancy-Ga donor complex ($V_{Cd}{}^{2-}D^{+}$).

IV. CONCLUDING REMARKS

The results reported in this paper demonstrate that piezomodulation and photomodulation of reflectivity or transmission bring out unique signatures in the spectrum. They provide a versatile, nondestructive experimental technique for studying features significant for a proper understanding of the electron band structure besides being valuable for sample characterization. Indeed these modulation techniques are particularly valuable in the study of semiconductor heterostructures as we have shown in our recent reports on DMS quantum-well structures,[47] ZnSe epilayer on GaAs,[8,48] and quantum-well structures consisting of $GaAs/Al_xGa_{1-x}As$,[49] all fabricated by molecular-beam epitaxy, and DMS epilayers grown by liquid-phase epitaxy.[8,50]

The observation of a clear signature associated with the spin-orbit-split Γ_7 band in $Cd_{1-x}Mn_xTe$ reported in this paper opens the way for a study of its behavior under a magnetic field; the associated p-d exchange interaction is of fundamental interest in a full understanding of the magnetization of DMS's. Work along these lines is in progress.

ACKNOWLEDGMENTS

We thank Dr. K. C. Hass for stimulating discussions and Professor J. K. Furdyna and Ms. U. Debska for the samples used in the investigation. The work was supported in part by the National Science Foundation under Grant No. DMR-85-20866. The work carried out at the Francis Bitter National Magnet Laboratory was supported by the National Science Foundation Grant No. DMR-86-16787 (A.K.R. and Y.R.L.) and Grant No. DMR-85-04366 (R.L.A.).

[1]J. K. Furdyna, J. Appl. Phys. **53**, 7637 (1982); A. K. Ramdas, *ibid.* **53**, 7649 (1982).

[2]R. L. Aggarwal, S. N. Jasperson, Y. Shapira, S. Foner, T. Sakakibara, T. Goto, N. Miura, K. Dwight, and A. Wold, in *Proceedings of the 17th International Conference on the Physics of Semiconductors, San Francisco, 1984,* edited by J. D. Chadi and W. A. Harrison (Springer-Verlag, New York, 1985), p. 1419; R. L. Aggarwal, S. N. Jasperson, P. Becla, and R. R. Galazka, Phys. Rev. B **32**, 5132 (1985); Y. Shapira, S. Foner, P. Becla, D. N. Domingues, M. J. Naughton, and J. S. Brooks, *ibid.* **33**, 356 (1986).

[3]D. U. Bartholomew, E.-K. Suh, S. Rodriguez, A. K. Ramdas, and R. L. Aggarwal, Solid State Commun. **62**, 235 (1987).

[4]L. M. Corliss, J. M. Hastings, S. M. Shapiro, Y. Shapira, and P. Becla, Phys. Rev. B **33**, 608 (1986); T. M. Giebultowicz, J. J. Rhyne, and J. K. Furdyna, J. Appl. Phys. **61**, 3537 (1987).

[5]R. R. Galazka, Shoichi Nagata, and P. H. Keesom, Phys. Rev. B **22**, 3344 (1980); P. H. Keesom, *ibid.* **33**, 6512 (1986); W. J. M. DeJonge, A. Twardowski, and C. J. M. Denissen, in *Proceedings of the Materials Research Society Symposium on Diluted Magnetic (Semimagnetic) Semiconductors, Boston, 1986,* edited by R. L. Aggarwal, J. K. Furdyna, and F. von Molnar (Materials Research Society, Boston, 1987), p. 153.

[6]S. Venugopalan, A. Petrou, R. R. Galazka, A. K. Ramdas, and S. Rodriguez, Phys. Rev. B **25**, 2681 (1982).

[7]Preliminary reports of our work have appeared in Y. R. Lee and A. K. Ramdas, Solid State Commun. **51**, 861 (1984); Y. R. Lee, A. K. Ramdas, and R. L. Aggarwal, in *Proceedings of the 18th International Conference on the Physics of Semiconductors, Stockholm, 1986,* edited by O. Engström (World Scientific, Singapore, 1987), p. 1759.

[8]Y. R. Lee, Ph.D. thesis, Purdue University, 1987 (unpublished).

[9]Perkin-Elmer Corporation, Norwalk, CT 06856.

[10]Channel Industries Inc., 839 Ward Drive, Santa Barbara, CA 93111.

[11]See, for example, R. E. Nahory and J. L. Shay, Phys. Rev. Lett. **21**, 1569 (1968). Monochromatic radiation from a laser with photon energy larger than that of the fundamental ener-

gy gap of the sample generates nonequilibrium free carriers which, in turn, produce a space charge field near the surface. The electromodulatedlike reflectivity spectra can thus be obtained without the complications associated with attaching electrical contacts necessary in the conventional electromodulation experiments.

[12]J. Camassel, D. Auvergne, H. Mathieu, R. Triboulet, and Y. Marfaing, Solid State Commun. **13**, 63 (1973).

[13]For crystal structure, see R. W. G. Wyckoff, *Crystal Structures* (Interscience, New York, 1960), Chap. III. For energy gap, see J. W. Allen, G. Lucovsky, and J. C. Mikkelson, Jr., Solid State Commun. **24**, 367 (1977); M. Podgòrny and J. Oleszkiewicz, J. Phys. C **16**, 2547 (1983).

[14]B. Montegu, A. Laugier, and R. Triboulet, J. Appl. Phys. **56**, 3061 (1984).

[15]N. Bottka, J. Stankiewicz, and W. Giriat, J. Appl. Phys. **52**, 4189 (1981).

[16]For a complete review, see M. L. Cohen and D. J. Chadi, in *Handbook of Semiconductors,* edited by T. S. Moss (North-Holland, New York, 1980), Vol. 2, p. 155.

[17]J. K. Furdyna, J. Vac. Sci. Technol. A **4**, 2002 (1986).

[18]D. L. Peterson, A. Petrou, W. Giriat, A. K. Ramdas, and S. Rodriguez, Phys. Rev. B **33**, 1160 (1986).

[19]Y. P. Varshni, Physica **34**, 149 (1967).

[20]C. Z. Van Doorn and D. de Nobel, Physica **22**, 338 (1956).

[21]D. de Nobel, Philips Res. Rep. **14**, 361 (1959).

[22]W. Giriat and J. Stankiewicz, Phys. Status Solidi B **124**, K53 (1984).

[23]See K. Zanio, in *Semiconductors and Semimetals,* edited by R. K. Willardson and A. C. Beer (Academic, New York, 1978), Vol. 13, p. 85.

[24]T. Kendelewicz, Solid State Commun. **36**, 127 (1980).

[25]R. Bücker, H.-E. Gumlich, and M. Krause, J. Phys. C **18**, 661 (1985).

[26]J. Stankiewicz, Phys. Rev. B **27**, 3631 (1983).

[27]A. Twardowski, T. Dietl, and M. Demianiuk, Solid State Commun. **48**, 845 (1983).

[28]R. B. Bylsma, W. M. Becker, J. Kossut, U. Debska, and D. Yoder-Short, Phys. Rev. B **33**, 8207 (1986).

[29]J. Diouri, J. P. Lascaray, and M. El Amrani, Phys. Rev. B **31**, 7995 (1985).

[30]R. Y. Tao, M. M. Moriwaki, W. M. Becker, and R. R. Galazka, J. Appl. Phys. **53**, 3772 (1982).

[31]A. Franciosi, Shu Chang, R. Reifenberger, U. Debska, and R. Riedel, Phys. Rev. B **32**, 6682 (1985).

[32]M. Taniguchi, L. Ley, R. L. Johnson, J. Ghijsen, and M. Cardona, Phys. Rev. B **33**, 1206 (1986).

[33]B. E. Larson, K. C. Hass, H. Ehrenreich, and A. E. Carlsson, Solid State Commun. **56**, 347 (1985).

[34]A. Twardowski, M. Nawrocki, and J. Ginter, Phys. Status Solidi B **96**, 497 (1979).

[35]Y. R. Lee, A. K. Ramdas, and R. L. Aggarwal, Phys. Rev. B **33**, 7383 (1986).

[36]J. Calas, J. P. Lascaray, M. Averous, F. El Darazi, and D. Coquillat, Solid State Commun. **54**, 371 (1985).

[37]S.-H. Wei and A. Zunger, Phys. Rev. B **35**, 2340 (1987).

[38]H. Ehrenreich, K. C. Hass, N. F. Johnson, B. E. Larson, and R. J. Lempert, in *Proceedings of the 18th International Conference on the Physics of Semiconductors, Stockholm, 1986,* edited by O. Engström (World Scientific, Singapore, 1986), p. 1751.

[39]A. Franciosi, A. Wall, Y. Gao, J. H. Weaver, M.-H. Tsai, J. D. Dow, R-V. Kasowski, R. Reifenberger, and F. Pool (unpublished).

[40]D. U. Batholomew, J. K. Furdyna, and A. K. Ramdas, Phys. Rev. B **34**, 6943 (1986).

[41]E. Müller, W. Gebhardt, and W. Rehwald, J. Phys. C **16**, L1141 (1983).

[42]G. Ambrazevičius, G. Babonas, S. Marcinkevičius, V. D. Prochukhan, and Yu. V. Rud, Solid State Commun. **49**, 651 (1984).

[43]J. E. Morales Toro, Ph.D. thesis, Purdue University, 1985 (unpublished).

[44]D. Langer and S. Ibuki, Phys. Rev. **138**, A809 (1965).

[45]J. E. Morales Toro, W. M. Becker, B. I. Wang, U. Debska, and J. W. Richardson, Solid State Commun. **52**, 41 (1984).

[46]T. Kendelewicz, Solid State Commun. **36**, 162 (1980).

[47]R. L. Harper, S. Hwang, N. C. Giles, R. N. Bicknell, J. F. Schetzina, Y. R. Lee, and A. K. Ramdas, J. Vac. Sci. Technol. A **6**, 2627 (1988).

[48]Y. R. Lee, A. K. Ramdas, L. A. Kolodziejski, and R. L. Gunshor, Phys. Rev. B (to be published).

[49]Y. R. Lee, A. K. Ramdas, F. A. Chambers, J. M. Meese, and L. R. Ram Mohan, Appl. Phys. Lett. **50**, 600 (1987).

[50]L. X. Li, Y. R. Lee, A. K. Ramdas, and J. K. Furdyna (unpublished).